

2014

Altered mechanobiology of Schlemm's canal endothelial cells in glaucoma

Darryl R. Overby
Imperial College London

Enhua H. Zhou
Novartis Institutes of BioMedical Research


Rocio Vargas-Pinto
Imperial College London

Ryan M. Pedrigi
University of Nebraska-Lincoln, rpedrigi@unl.edu

Rudolf Fuchshofer
Universitat Regensburg

See next page for additional authors

Follow this and additional works at: <http://digitalcommons.unl.edu/mechengfacpub>

 Part of the [Mechanics of Materials Commons](#), [Nanoscience and Nanotechnology Commons](#), [Other Engineering Science and Materials Commons](#), and the [Other Mechanical Engineering Commons](#)

Overby, Darryl R.; Zhou, Enhua H.; Vargas-Pinto, Rocio; Pedrigi, Ryan M.; Fuchshofer, Rudolf; Braakman, Sietse T.; Gupta, Ritika; Perkumas, Kristin M.; Sherwood, Joseph M.; Vahabikashi, Amir; Dang, Quynh; Kim, Jae Hun; Ethier, C. Ross; Stamer, W. Daniel; Fredberg, Jeffrey J.; and Johnson, Mark, "Altered mechanobiology of Schlemm's canal endothelial cells in glaucoma" (2014). *Mechanical & Materials Engineering Faculty Publications*. 297.
<http://digitalcommons.unl.edu/mechengfacpub/297>

This Article is brought to you for free and open access by the Mechanical & Materials Engineering, Department of at DigitalCommons@University of Nebraska - Lincoln. It has been accepted for inclusion in Mechanical & Materials Engineering Faculty Publications by an authorized administrator of DigitalCommons@University of Nebraska - Lincoln.

Authors

Darryl R. Overby, Enhua H. Zhou, Rocio Vargas-Pinto, Ryan M. Pedrigi, Rudolf Fuchshofer, Sietse T. Braakman, Ritika Gupta, Kristin M. Perkumas, Joseph M. Sherwood, Amir Vahabikashi, Quynh Dang, Jae Hun Kim, C. Ross Ethier, W. Daniel Stamer, Jeffrey J. Fredberg, and Mark Johnson

Altered mechanobiology of Schlemm's canal endothelial cells in glaucoma

Darryl R. Overby^{a,1}, Enhua H. Zhou^{b,1,2}, Rocio Vargas-Pinto^{c,1}, Ryan M. Pedrigi^a, Rudolf Fuchshofer^d, Sietse T. Braakman^a, Ritika Gupta^a, Kristin M. Perkumas^e, Joseph M. Sherwood^a, Amir Vahabikashi^c, Quynh Dang^b, Jae Hun Kim^b, C. Ross Ethier^{a,f,g}, W. Daniel Stamer^{e,h}, Jeffrey J. Fredberg^b, and Mark Johnson^{c,i,3}

^aDepartment of Bioengineering, Imperial College London, London SW7 2AZ, United Kingdom; ^bProgram in Molecular and Integrative Physiological Sciences, Department of Environmental Health, Harvard School of Public Health, Boston, MA 02115; ^cDepartment of Biomedical Engineering, Northwestern University, Evanston, IL 60208; ^dInstitute of Human Anatomy and Embryology, Universität Regensburg, 93053 Regensburg, Germany; ^eDepartment of Ophthalmology, Duke University, Durham, NC 27710; ^fWallace H. Coulter Department of Biomedical Engineering, Georgia Institute of Technology, Atlanta, GA 30332; ^gDepartments of Biomedical Engineering and Ophthalmology, Emory University, Atlanta, GA 30322; ^hDepartment of Biomedical Engineering, Duke University, Durham, NC 27710; and ⁱDepartments of Mechanical Engineering and Ophthalmology, Northwestern University, Evanston, IL 60208

Edited by David A. Weitz, Harvard University, Cambridge, MA, and approved August 18, 2014 (received for review June 9, 2014)

Increased flow resistance is responsible for the elevated intraocular pressure characteristic of glaucoma, but the cause of this resistance increase is not known. We tested the hypothesis that altered biomechanical behavior of Schlemm's canal (SC) cells contributes to this dysfunction. We used atomic force microscopy, optical magnetic twisting cytometry, and a unique cell perfusion apparatus to examine cultured endothelial cells isolated from the inner wall of SC of healthy and glaucomatous human eyes. Here we establish the existence of a reduced tendency for pore formation in the glaucomatous SC cell—likely accounting for increased outflow resistance—that positively correlates with elevated subcortical cell stiffness, along with an enhanced sensitivity to the mechanical microenvironment including altered expression of several key genes, particularly connective tissue growth factor. Rather than being seen as a simple mechanical barrier to filtration, the endothelium of SC is seen instead as a dynamic material whose response to mechanical strain leads to pore formation and thereby modulates the resistance to aqueous humor outflow. In the glaucomatous eye, this process becomes impaired. Together, these observations support the idea of SC cell stiffness—and its biomechanical effects on pore formation—as a therapeutic target in glaucoma.

cell mechanics | primary open-angle glaucoma | modulus | cytoskeleton

Aqueous humor flows across the inner wall endothelium of Schlemm's canal (SC) and generates a transendothelial pressure gradient from the cellular base to the cellular apex. From a biomechanical perspective, the direction of this gradient is remarkable considering that the endothelium of the systemic vasculature experiences a pressure gradient in precisely the opposite direction. In the healthy eye, this basal-to-apical trans-cellular pressure gradient is of sufficient magnitude to partially separate the SC cell from its supporting basement membrane, inflate dome-shaped structures known as giant vacuoles, and generate cellular mechanical strains exceeding 50% (Fig. 1) (1). The formation of giant vacuoles leads to substantial thinning of the SC endothelial cell and is thought to be associated with formation of pores that provide an outflow pathway across the SC endothelium (2). Although reported dysfunction of the pore formation process might be expected to affect outflow resistance and elevate intraocular pressure (IOP) (3, 4), mechanisms for such dysfunction have never before been established, in large part because SC cells from healthy eyes are so difficult to isolate technically, but also because isolated SC cells from the glaucomatous eye are a resource that has been exceedingly scarce. Here for the first time to our knowledge we show that the process of pore formation differs substantially between cells from the healthy versus the glaucomatous human eye and show, further, that this difference depends upon cytoskeletal stiffness that is altered in the glaucomatous SC cell, likely owing to altered

substrate sensitivity and gene expression in these cells. Specifically, stiffer glaucomatous cells impede pore formation and thereby elevate IOP.

Results

Pore Formation in SC Cells Is Altered in Glaucomatous Cell Strains. To examine pore formation in SC cells, we used an in vitro monolayer perfusion system to mimic the biomechanical and filtration environment of SC endothelium in vivo (5). As described previously, SC cells were isolated from normal and glaucomatous human donors and extensively characterized (*Materials and Methods*) (6, 7). When perfused in a basal-to-apical direction pores formed in SC cell monolayers, with pores passing trans-cellularly through individual SC cells or paracellularly between neighboring SC cells, consistent with the two pore types observed along the SC endothelium in situ (Fig. 2A) (8). The density of pores (pores per cell area) increased significantly with perfusion pressure ($P < 3 \times 10^{-5}$; Fig. 2B), and porosity (pore area per cell area) showed a similar dependence upon pressure ($P < 0.003$;

Significance

Glaucoma is a leading cause of blindness. The elevated intraocular pressure characteristic of many cases of glaucoma is attributable to increased resistance to aqueous humor outflow. However, the cause of this increased flow resistance has eluded investigators for over 140 y. Here we demonstrate that cells from the canal of Schlemm of glaucomatous eyes have altered gene expression and increased cytoskeletal stiffness that leads to reduced pore formation in these cells, likely accounting for increased outflow resistance associated with glaucoma. These findings thus establish that dysfunctional cytoskeletal mechanics may lie at the heart of this disease process and thereby motivate development of glaucoma therapeutics that target cell stiffness.

Author contributions: D.R.O., E.H.Z., R.V.-P., R.M.P., R.F., S.T.B., A.V., C.R.E., W.D.S., J.J.F., and M.J. designed research; E.H.Z., R.V.-P., R.M.P., R.F., S.T.B., R.G., K.M.P., A.V., Q.D., and J.H.K. performed research; D.R.O., E.H.Z., R.V.-P., K.M.P., J.M.S., J.H.K., W.D.S., J.J.F., and M.J. contributed new reagents/analytic tools; D.R.O., E.H.Z., R.V.-P., R.M.P., R.F., S.T.B., R.G., K.M.P., J.M.S., A.V., J.H.K., C.R.E., W.D.S., J.J.F., and M.J. analyzed data; and D.R.O., E.H.Z., R.V.-P., R.M.P., R.F., S.T.B., J.M.S., A.V., C.R.E., W.D.S., J.J.F., and M.J. wrote the paper.

The authors declare no conflict of interest.

This article is a PNAS Direct Submission.

Freely available online through the PNAS open access option.

¹D.R.O., E.H.Z., and R.V.-P. contributed equally to this work.

²Present address: Ophthalmology, Novartis Institutes of BioMedical Research, Cambridge, MA 02139.

³To whom correspondence should be addressed. Email: m-johnson2@northwestern.edu.

This article contains supporting information online at www.pnas.org/lookup/suppl/doi:10.1073/pnas.1410602111/-DCSupplemental.

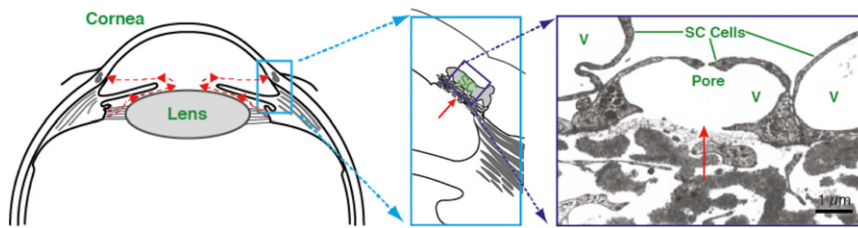


Fig. 1. Aqueous humor flow pathway. (Left) Schematic of anterior segment of eye showing the direction of aqueous humor flow in red. (Center) Enlargement of the iris-cornea angle (boxed region in left panel) to show the conventional outflow pathway. (Right) Transmission electron micrograph of endothelial cells forming the inner wall of SC; aqueous humor crosses the endothelium through pores to enter the lumen of SC. V, giant vacuoles. C is reproduced with permission from ref. 41.

online supplement). The increase in pore density with perfusion pressure was observed for both transcellular and paracellular pores ($P < 0.005$; *SI Text*). Apical-to-basal perfusion of these monolayers showed no such dependence of pore density (Fig. 2B) or porosity (*SI Text*) on perfusion pressure, consistent with previous studies showing rectified flow across this endothelium and its role as part of the blood–aqueous barrier (9).

Compared with the pore density measured in normal SC cell strains perfused in a basal-to-apical direction at 6 mmHg, pore density in glaucomatous SC cell strains was markedly reduced; pore density in glaucomatous cells was threefold smaller and the difference was highly statistically significant ($P < 2 \times 10^{-4}$; Fig. 2C). Pore density seen in glaucomatous SC cell strains perfused at 6 mmHg was comparable to unperfused normal controls (Fig. 2B and C). Porosity was similarly reduced in glaucomatous SC cells compared with SC cells from normal eyes ($P < 0.04$; *SI Text*) and was attributable to a reduction in transcellular and paracellular pores, although neither alone achieved statistical significance.

Glaucomatous SC Cells Demonstrate Elevated Subcortical Stiffness. We reasoned that it would be more difficult for a pore to form in stiffer SC cells. To investigate this possibility, we measured the stiffness of SC cells isolated from normal and glaucomatous human donors (*Materials and Methods*) using atomic force microscopy (AFM) using both sharp tips (20-nm tip radius) and rounded tips (4.5 μm and 10 μm) (10). In other cellular systems, AFM measurements using a sharp tip characterize the cell cortex, whereas larger, spherical tips probe the subcortical cytoskeleton (10). Here we use the term “cortex” to refer to the actin-dense region of the cell lying immediately beneath the plasma membrane, and the term “subcortical cytoskeleton” to refer to the internal cytoskeleton underlying the cortex (11). For all tip geometries, elastic moduli were found to be similar between nuclear and peripheral regions of the cell, and there was no systematic variation between Young’s modulus and donor age (*SI Text*). Cell stiffness measured with sharp tips was 10-fold higher than that measured with the larger, spherical tips (Fig. 3B), consistent with the prominent actin-rich cell cortex found in SC cells and other endothelia (Fig. 3A).

Measured with a sharp AFM tip, we found no difference in stiffness between normal versus glaucomatous SC cells ($P > 0.85$; Fig. 3B). Cortex thickness as measured by structured illumination microscopy was similar between normal (400 ± 20 nm, $n = 3$ cell strains) and glaucomatous SC cells (380 ± 60 nm, $n = 2$). However, when measured with the larger, spherical AFM tips, we found systematic differences in stiffness between glaucomatous SC versus normal SC cells (Fig. 3B and C). With a 4.5- μm tip, the modulus of glaucomatous SC cells was 1.47 ± 0.29 kPa ($n = 5$ cell strains; $m = 128$ measurements), whereas that of normal SC cells was measured as 1.01 ± 0.12 kPa ($n = 6$; $m = 104$) ($P < 0.12$). Using a 10- μm tip, the modulus of glaucomatous SC cells was 1.24 ± 0.11 kPa ($n = 5$; $m = 120$), whereas that of normal SC cells was 0.79 ± 0.10 kPa ($n = 6$; $m = 153$) ($P < 0.02$). Relative to the normal SC cells, glaucomatous SC cells revealed substantially elevated subcortical stiffness. Both cortical and subcortical SC cell stiffness were greatly reduced by latrunculin-A, consistent with an important role for actin in determining stiffness (Fig. 3A); however, there was no difference in the relative decrease in cell stiffness following latrunculin between

normal and glaucomatous SC cells (*SI Text*), suggesting that perhaps another constituent of the subcortical cytoskeleton [e.g., intermediate filaments (11)] may be altered in glaucomatous SC cells.

For two normal and three glaucomatous SC cell strains in which both cell stiffness and pore density were measured we examined the relationship between these parameters. Subcortical stiffness (10- μm spherical tip) was related inversely to pore density ($P < 0.002$; Fig. 3D) and porosity ($P < 0.012$; *SI Text*). A relationship was apparent between subcortical stiffness and pore density for both pore subtypes; however, subcortical stiffness showed a more significant correlation with transcellular pore density ($P < 0.02$) compared with paracellular pore density ($P < 0.07$) (*SI Text*). These data do not establish causality but do strongly support the idea that increased subcortical cell stiffness and decreased pore formation go hand in hand.

On Increasingly Stiffer Gels, Both Normal and Glaucomatous SC Cells Stiffen. We asked next what might cause this stiffness difference. One possibility is mechanotransduction of the mechanical properties of the SC cell microenvironment (12, 13). We thus investigated how substrate stiffness might influence SC cell

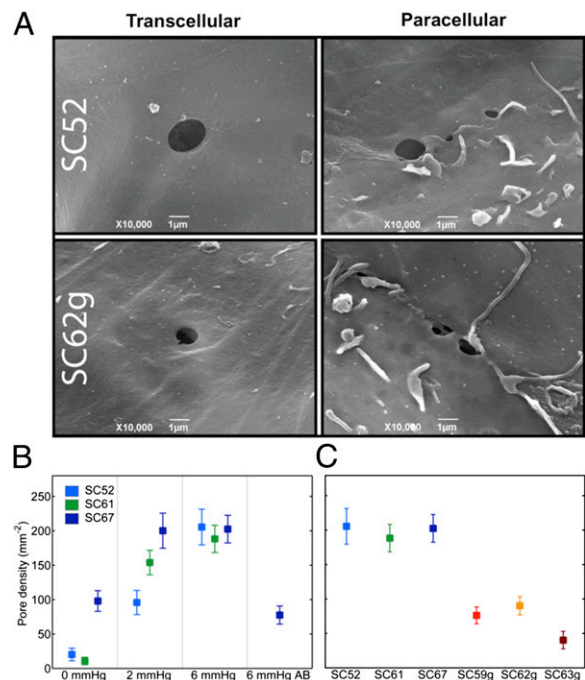


Fig. 2. Pore density in perfused SC monolayers. (A) Representative image of transcellular and paracellular pores in normal (SC52) and glaucomatous SC (SC62g) cells. (B) Pore density increases in monolayers formed from three nonglaucomatous SC cell strains with transcellular (basal-to-apical) pressure drop; in one SC cell strain (SC67) perfused in the apical-to-basal direction (AB), pore densities are similar to unperfused controls at 0 mmHg. (C) Pore density is reduced in glaucomatous compared with normal SC cells following perfusion at 6 mmHg in the basal-to-apical direction. Bars are SEM.

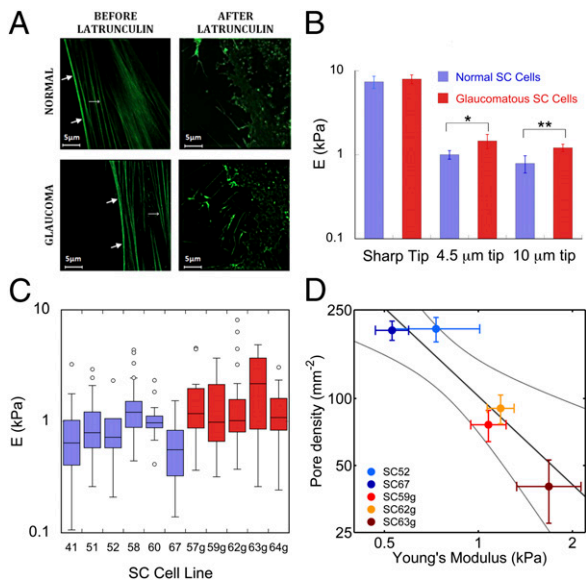


Fig. 3. Young's modulus for normal and glaucomatous SC cells as measured by AFM. (A) Structured illumination microscopy images of normal and glaucomatous SC cells labeled with actin filament marker (42) rAV-LifeAct-TagGFP2 before and after application of latrunculin-A. Thick arrows, cortex; thin arrows, stress fibers. (B) Median and SEs of the modulus of six normal (blue) and five glaucomatous (red) nonconfluent SC cell strains as measured with three different AFM tips. Modulus is determined from force-deformation curves using a modified Hertzian analysis (10); * $P = 0.117$, ** $P = 0.017$. (C) Box and whisker plot (43) of individual AFM measurements of cell modulus using a 10- μm tip for each of the six normal and five glaucomatous SC cell strains examined. (D) There is a significant correlation (dark line) between pore density and the modulus of the subcortical cytoskeleton, as measured by AFM using a 10- μm spherical tip. Bars represent SEM on pore density and modulus. Light curves in D represent 95% confident intervals on the slope of the GLM linear regression.

stiffness and gene expression. Because of the need to examine a large number of cells on substrates of a variety of stiffnesses, we used optical magnetic twisting cytometry (OMTC) (*Materials and Methods*) to study SC cells isolated from normal and glaucomatous human donors (*Materials and Methods*).

Grown on rigid substrates, we found no difference in stiffness between normal and glaucomatous SC cells strains (*SI Text*), and, as expected, these results were consistent with the AFM findings using a sharp tip described above (11, 14). We also examined how SC cells grown on rigid substrates responded to drugs with known effects on outflow resistance. Similar to our finding previously reported for normal SC cells (15), we found in glaucomatous SC cells that every agent that we examined that decreased outflow resistance also decreased cell stiffness, and every agent that increased outflow resistance also increased cell stiffness (*SI Text*).

We then examined the influence of substrate stiffness on the cells. The physiological substrate of the SC cell is the trabecular meshwork, and its compressive Young's modulus has been reported to be substantially increased in glaucoma (16). Normal and glaucomatous SC cells were cultured on collagen-coated polyacrylamide gels of tunable stiffness (*Materials and Methods*) with Young's moduli ranging from 1.1 kPa to 34.4 kPa, the former mimicking normal trabecular meshwork and the latter mimicking glaucomatous trabecular meshwork (albeit not modeling the complex geometry of the basement membrane and juxtacanalicular connective tissue that underlie the SC cells).

With increasing gel stiffness SC cells exhibited more prominent actin stress fibers and vinculin-containing focal adhesions (compare Fig. 4 A and B), suggestive of increased cytoskeletal contractility and/or elevated cell stiffness. OMTC measurements

showed that normal SC cells stiffened in response to increased substrate stiffness ($P = 10^{-6}$; Fig. 4 C and D) and were 131% stiffer when cultured on the stiffest gel compared with the softest gel. Glaucomatous SC cells showed a much greater stiffening response ($P = 0.011$ comparing normal versus glaucoma), increasing by 371% over the same range of substrate stiffness (Fig. 4 E and F). Thus, similar to other endothelial cells, SC endothelial cells stiffen in response to increasing substrate stiffness. Compared with the healthy SC cell, the glaucomatous SC cell exhibits a strikingly enhanced stiffening response.

Expression of Glaucoma-Related Genes Is Dependent upon Substrate Stiffness and Exaggerated in Glaucomatous Cell Strains. In endothelial cells and fibroblasts, substrate stiffness is known to modulate gene expression (17–19). Using real-time quantitative PCR as a function of substrate stiffness in normal and glaucomatous SC cells (*Materials and Methods*), we examined the expression levels of 13 genes (Table 1) previously linked to mechanosensing, glaucoma, ECM remodeling, or TGF- β 2/connective tissue growth factor (CTGF) signaling.

The mRNA expression of *Colla1* was up-regulated by up to 20-fold with increasing substrate stiffness for both normal and glaucomatous cells ($P < 10^{-9}$), with no significant difference between normal and glaucomatous cells ($P > 0.4$) (Fig. 5A) (see *Materials and Methods* for statistical treatment). Significant

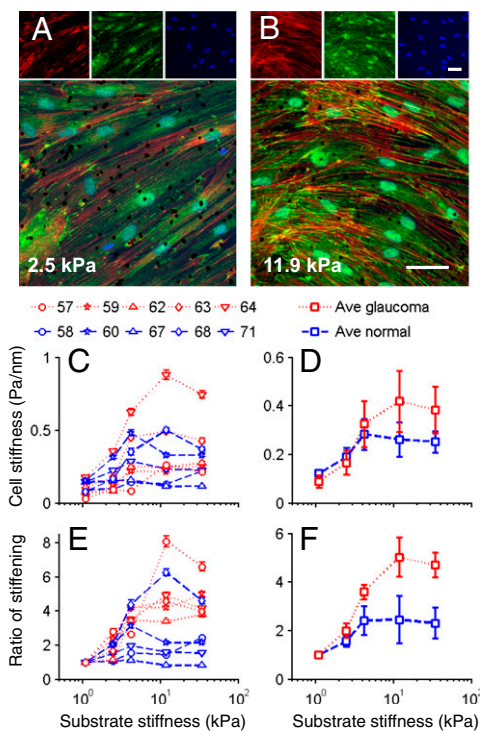


Fig. 4. Influence of substrate stiffness on the biomechanical properties of SC cells. As the substrate stiffness increases, the stiffness of SC cells increases by different amounts in a donor- and disease-dependent manner. (A and B) Fluorescent micrographs of normal SC cells labeled for f-actin (red), vinculin (green), and DNA (blue) at two levels of substrate stiffness; black dots are 4.5- μm magnetic beads used for OMTC. (Scale bars: 50 μm .) (C and D) Cell stiffness index (g) of normal (blue) and glaucomatous (red) SC cells as measured by OMTC for individual cell strains (numbers above figure indicate cell strain) (C) or averages over all cell strains (D). (E and F) Stiffness index normalized by the value at the lowest substrate stiffness, expressed for individual cell strains (E) or averages over all cell strains (F). Median \pm SEM with $n > 600$ beads for C and E; mean \pm SEM with $n = 5$ cell strains each for D and F. Note that because the embedding depth of the beads in the cells is not known, an index of cell stiffness, g , is presented rather than an absolute value (44).

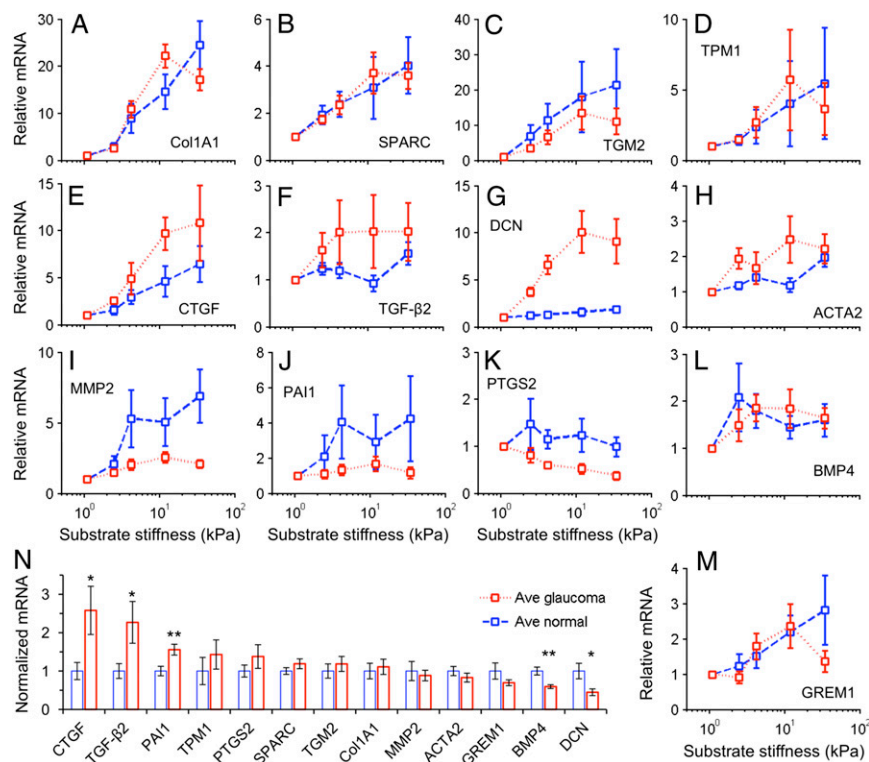


Fig. 5. Increases in substrate stiffness modulated SC cell gene expression. (A–M) The increases in substrate stiffness expression levels in normal or glaucomatous cell strains relative to that on the softest gel of that cell strain. Increased substrate stiffness led to increased expression in all genes except *PTGS2* that showed constant or decreased expression. (N) The expression levels of 13 genes averaged across substrate stiffness and across donors were compared between normal and glaucomatous cell strains, normalized to the averaged expression level in the normal cells on the softest gel. Statistically significant differences between normal and glaucomatous cells indicated by * $P < 0.05$ and ** $P < 0.01$. Mean \pm SEM with $n = 5$ for A–M; mean \pm SEM with $n = 25$ for N.

increases with increasing substrate stiffness were also seen for *SPARC* ($P < 10^{-6}$), *TGM2* ($P < 10^{-4}$), *ACTA2* ($P < 10^{-5}$), *MMP2* ($P < 10^{-4}$), *PAI1* ($P < 0.005$), *BMP4* ($P < 10^{-4}$), and *GREM1* ($P < 10^{-5}$) (Fig. 5 B, C, H–J, L, and M). Marginally statistically significant increases ($0.01 < \text{overall } P < 0.05$) in *TPM1* and *TGF-β2* were observed with increasing substrate stiffness (Fig. 5 D and F). These results indicate that normal and glaucomatous SC cells share some common molecular responses to elevated substrate stiffness.

We also identified three genes that were differentially modulated by substrate stiffness in glaucomatous compared with normal SC cells. *PTGS2* had a marginally significant negative association with substrate stiffness in glaucomatous cells (overall $P < 0.03$) but not in normal cells (Fig. 5K). Importantly, *CTGF* and *DCN* were more strongly up-regulated by elevated substrate stiffness in glaucomatous SC cells ($P < 0.05$, $P < 10^{-3}$, respectively) than in normals (Fig. 5 E and G). Of note, the absolute increase in *CTGF* gene expression in glaucomatous cell strains, compared with normals ($P < 0.05$), was the highest of all of the genes investigated (Fig. 5N). Other genes with higher expression in glaucomatous SC cells included *TGF-β2* ($P < 0.05$) and *PAI1* ($P < 0.01$). Genes with lower expression in glaucomatous SC cells included *DCN* ($P < 0.05$) and *BMP4* ($P < 0.01$).

Together, these data demonstrate that SC cells modulate their gene expression in tandem with substrate stiffness and that glaucomatous SC cells have altered substrate sensitivity that affects key genes, particularly *CTGF* and *DCN*. In a mouse model of glaucoma, *CTGF* has been associated with increased stress fiber formation, IOP elevation, and glaucomatous optic neuropathy (20). Here we establish a link between the expression of these same genes and changes of substrate stiffness.

Discussion

The cause of the elevated pressure and increased outflow resistance characteristic of glaucoma is unknown despite being a topic of investigation for over 140 y (21). Recent studies have focused on the role of decreased extracellular matrix permeability (22) or increased extracellular matrix stiffness (16) in the glaucomatous process. Our studies here suggest that the cells of

the inner wall of SC may play a fundamental role in generating increased outflow resistance in the diseased eye. The density of pores in glaucomatous eyes is lower than in normal eyes (3, 4). Pores in the inner wall endothelium of SC are thought to modulate aqueous outflow resistance through a hydrodynamic interaction with the flow of aqueous humor passing through the trabecular meshwork (23, 24). Thus, decreased pore density is expected to increase the resistance to outflow of aqueous humor from the eye and thereby increase IOP, a characteristic of many cases of glaucoma. Moreover, in the glaucomatous eye the ultrastructure and material properties of the trabecular meshwork that supports the SC cell are altered (16, 25, 26). Because SC cells from glaucomatous human eyes comprise a scarce experimental resource, an innate limitation of this study is that the differences reported between normal versus glaucomatous SC cells may be inherent to the disease process itself or may arise instead from chronic exposure to drugs used to treat the disease. Although we cannot distinguish between these possibilities, we do establish that these glaucomatous SC cells exhibit elevated subcortical cell stiffness, enhanced sensitivity to the mechanical

Table 1. Genes investigated and the proteins they code for

Gene	Protein
<i>ACTA2</i>	Alpha smooth muscle actin (SMA)
<i>Col1A1</i>	α -1 type I collagen
<i>CTGF</i>	Connective tissue growth factor
<i>DCN</i>	Decorin
<i>MMP2</i>	Matrix metalloproteinase-2
<i>PAI1</i>	Plasminogen activator inhibitor-1
<i>PTGS2</i>	Prostaglandin-endoperoxide synthase 2 (COX-2)
<i>SPARC</i>	Secreted protein acidic and rich in cysteine
<i>TGF-β2</i>	Transforming growth factor-β2
<i>TGM2</i>	Tissue transglutaminase
<i>TPM1</i>	Tropomyosin α -1 chain
<i>BMP4</i>	Bone morphogenetic protein 4
<i>GREM1</i>	Gremlin 1

Table 2. Summary of SC cell strain donor ages used in the present study

Gene	Cell strain no.	Donor age, y
Normal	SC41	64
	SC51	66
	SC52	71
	SC58	34
	SC60	58
	SC61	88
	SC67	44
	SC68	30
	SC71	44
	Glaucoma	SC57g
SC59g		55
SC62g		66
SC63g		78
SC64g		78

microenvironment, and altered gene expression, notably *CTGF*, which has been shown to lead to ocular hypertension and glaucomatous optic neuropathy in mice (20). Furthermore, we have demonstrated that these altered material properties of the glaucomatous SC cells render them less able to form pores and thus presumably lead to increased IOP.

To lower IOP in glaucoma, two classes of new drugs are currently in clinical trials—Rho kinase inhibitors and actin depolymerizers (27, 28)—both of which lower outflow resistance (29, 30). The exact site of action in the conventional outflow tract of these drugs in lowering IOP in glaucoma is unknown, but it is interesting to note that both classes cause cell stiffness to decrease (15). We demonstrate here that both normal and glaucomatous SC cells alter their stiffness when treated with drugs that alter outflow resistance. These findings emphasize the importance of cell stiffness and the contractile state to the modulation of aqueous humor outflow resistance and control of IOP. The mechanosensitivity of SC cells thus represents an interesting therapeutic target for restoring the function of the conventional outflow pathway. Specifically, targeting SC cell stiffness is likely to provide an efficacious therapeutic approach to lower IOP for glaucoma therapy, with minimal off-target effects.

Materials and Methods

In the past, the comparison between normal and glaucomatous tissues and cells has been hindered by the lack of fresh human donor eyes. Our work included SC cells from nine normal and four glaucomatous donors, representing the largest collection of such samples to date (Table 2).

SC Cell Isolation and Culture. Human SC cells were isolated from cadaveric ocular tissue provided by Midwest Eye Bank, National Disease Research Interchange, or Life Legacy within 36 h of death with enucleation occurring less than 6 h after death. Isolation of cells from donor eye tissue was done according to techniques developed and optimized previously (6). Before use in experiments, all SC cell strains were characterized using three inclusion criteria: the expression of vascular endothelial cadherin, a net transendothelial electrical resistance of 10 ohms-cm² or greater, and the lack of myocilin induction by dexamethasone as described previously (7). We examined the change in cell stiffness with cell passaging and found no change through passage 6 (*SI Text*). A total of nine different cell strains isolated from nine donor eyes without a history of eye disease and five different cell strains isolated from four donors having a history of glaucoma were used in the present study (Table 2). For determination of ocular hypertension/glaucoma for eye donors, we relied on a combination of the following information provided to us by eye/tissue banks and/or analyses that were conducted on donor eyes once they were received in our laboratory: documentation of ocular hypertension/glaucoma history, presence of glaucoma eye drops on patient medication list, abnormally low outflow facility measurement of whole globes (<0.1 $\mu\text{L}\cdot\text{min}^{-1}\cdot\text{mmHg}^{-1}$ measured at time of receipt in the laboratory), and/or abnormally low axon counts (<500,000 axons per optic nerve).

SC Monolayer Perfusion and Pore Counting. SC monolayers were perfused and pore counts made following previously described methods (5, 8). Briefly, SC cells of passages 3–5 were seeded at confluence (4.5×10^4 cells/cm²) on track-etched filters and cultured for 2 d. SC cell layers were perfused in the basal-to-apical direction at 2 or 6 mmHg for 30 min with DMEM + 25 mM Hepes. Cell layers were then immersed in fixative while continuing perfusion with medium for an additional 30 min. For controls, cell layers were either not perfused and immersion-fixed at 0 mmHg or perfused in the opposite (apical-to-basal) direction at 6 mmHg followed by immersion in fixative. SC cell layers were processed and examined by scanning electron microscopy, pores were analyzed in 12 randomly selected regions (5,500 μm^2 each) per cell layer, and pore density and porosity (percentage area covered by pores) determined. Details are given in *SI Text*.

AFM. AFM measurements were made on subconfluent normal or glaucomatous SC cells at passage 4 or 5 with sharp pyramidal tips or spherical tips of diameter 4.5 or 10 μm using a Bioscope Catalyst atomic force microscope (Bruker). Young's modulus was determined using a modified Hertzian analysis (10). Studies with latrunculin-A used a concentration of 1 μM , with cells treated for 30 min.

Cortex and Cell Imaging. For imaging, SC cells were transduced with an adenovirus delivering an actin filament marker, rAV-LifeAct-TagGFP2 (*ibidi*). After 48 h of transduction, cells were washed with buffered saline. Cells were then imaged with a Nikon-structured illumination microscope before and after latrunculin-A treatment. Cortex thickness measurements were made from intensity profiles defining thickness as full width at half-maximum intensity. Cortex thickness was measured on roughly 10–25 cells of each cell strain and then averaged over the cell strains for three normal and two glaucomatous strains.

OMTC. Detailed descriptions and validations of OMTC have been given elsewhere (15, 31–33). Briefly, to probe the cortical cytoskeletal stiffness, ferrimagnetic beads (4.5- μm diameter) were coated with poly-L-lysine (PLL). The beads were allowed to attach to cells for 25–50 min. They were then magnetized with a strong magnetic pulse in the horizontal direction and twisted with a much weaker magnetic field in the vertical direction. This vertical field, which oscillates at 0.77 Hz, imposed a sinusoidal torque on each bead. The torque was automatically adjusted to achieve a median bead motion of about 60 nm. The bead motion was quantified by image analysis. The ratio of magnetic torque to bead motion defines the apparent stiffness (g^*) measured by each bead (34). g^* is a complex number and we report the modulus $g = |g^*|$, which has units of pascals per nanometer.

Fabrication of Substrates with Varied Stiffness and Testing Procedure. Published protocols were followed to make polyacrylamide gels composed of 8% (wt/vol) acrylamide, 3% (wt/vol) (3-acrylamidepropyl) trimethylammonium chloride (API), and a variable percentage of bisacrylamide (0.04, 0.1, 0.2, 0.5, and 1.3%; wt/vol) (18, 35–37). These API gels were positively charged and electrostatically absorb ECM proteins, including collagen 1 (36). Previous work confirmed the absorption of fibronectin and collagen to be independent of gel stiffness (38). Gels were cast between two glass plates to achieve a final thickness of about 0.8 mm. Disks 5 mm in diameter were punched out of gel sheets using surgical punches, transferred into 96-well plates, and stored in PBS. These gels were soaked in 10 $\mu\text{g}/\text{mL}$ collagen 1 overnight (PureCol; Advanced BioMatrix) before cell plating. Young's moduli of the gels were measured using AFM to be 1.1, 2.5, 4.2, 11.9, and 34.4 kPa for bisacrylamide concentrations of 0.04, 0.1, 0.2, 0.5, and 1.3%, respectively; the Young's modulus scaled roughly linearly with cross-linker concentration (*SI Text*). SC cells at passages 3–6 were seeded confluent (3×10^4 cells/cm²) on the gels, grown in low-glucose DMEM with 1% FBS for 3 d, and switched to DMEM with 1 \times ITS (Sigma-Aldrich) overnight before OMTC testing using PLL-coated beads. After OMTC twisting, the cells were directly lysed in trizol (Life Technologies) and stored frozen until real-time quantitative PCR measurements as described below.

Real-Time Quantitative RT-PCR. Structural integrity of RNA samples was confirmed by electrophoresis using 1% (wt/vol) agarose gels. First-strand cDNA was prepared from total RNA using the iScript cDNA Synthesis Kit (Bio-Rad) according to the manufacturer's instructions. Real-time RT-PCR was performed on a Bio-Rad iQ5 real-time PCR detection system (Bio-Rad) with the temperature profile as follows: 40 cycles of 10 s melting at 95 $^\circ\text{C}$, 40 s of annealing and extension at 60 $^\circ\text{C}$. All primer pairs (*SI Text*) extended over exon–intron boundaries. RNA that was not reverse-transcribed served as negative control for real-time RT-PCR. To allow for relative quantification, we identified housekeeping genes by using the software Genex (MultiD

Analysis) (39). In initial experiments, real-time RT-PCR for the potential housekeeping genes GNB2L1, GAPDH, and RPL32 was performed for each of the treatment protocols. Cycle threshold values were loaded to the software that distinguishes genes that are regulated in a specific condition from those that are very likely not. No differences were obtained between GAPDH and GNB2L1, so GNB2L1 was used for relative quantification of the real-time RT-PCR experiments. Quantification was performed using Bio-Rad iQ5 standard edition (Version 2.0.148.60623) software (Bio-Rad).

Statistical Methods. In general, the statistical analysis was done using SPSS (version 12.0; IBM). Because the cell stiffness for each donor is approximately log-normally distributed (SI Text), we reported it as median \pm SE, which was calculated based on logarithmically transformed data (34).

Regression analysis for the studies of the effect of substrate stiffness on cell stiffness and gene expression used the following relationship:

$$\frac{\text{Variable}(E_{\text{Substrate}})}{\text{Variable}(1.1 \text{ kPa})} - 1 = c_1 * \left(\frac{E_{\text{Substrate}}}{1.1 \text{ kPa}} - 1 \right) + c_2 * \left(\frac{E_{\text{Substrate}}}{1.1 \text{ kPa}} - 1 \right) * \text{Normal},$$

where $\text{Variable}(E_{\text{Substrate}})$ is the value of the parameter being measured (cell stiffness or gene expression) at a given value of substrate stiffness ($E_{\text{Substrate}}$). *Normal* is 1 for normal cell strains and 0 for glaucomatous cell strains. Correlations were taken as statistically significant when the correlation had an overall significance of $P < 0.01$ and either substrate stiffness and/or glaucoma affected the fit with $P < 0.05$ (unless otherwise noted). In all cases

where a statistically significant difference between glaucomatous cell strains and normals was reported, the addition of donor age as an additional covariate to the equation did not affect this conclusion (SI Text).

Because pore density is a discrete random variable comprising finite counts of sparse events, Poisson statistics were applied and an E-test (40) was used to compare Poisson-distributed pore densities between different perfusion pressures and between normal and glaucomatous SC cell strains. The generalized linear model (GLM) was used for regression analysis of pore density versus cell stiffness (as measured by AFM with a 10- μm spherical tip) applying a logarithmic link function. Differences in porosity were analyzed using a two-tailed two-sample Student *t* test. GLM analysis was also used for regression analysis of porosity versus cell stiffness with an identity link function.

ACKNOWLEDGMENTS. We gratefully acknowledge support from the National Glaucoma Research program of the Bright Focus Foundation; National Institutes of Health Grants R01 EY 01969, R21 EY018373, and T32 EY007128; the Whitaker International Scholars Program; the Deutsche Forschungsgemeinschaft (FOR 1075, TP3); the Georgia Research Alliance; and the Royal Society Wolfson Research Excellence Award. Northwestern University's Atomic and Nanoscale Characterization Experimental Center (used for atomic force microscopy studies) is supported by the National Science Foundation-Nanoscale Science and Engineering Center, the National Science Foundation-Materials Research Science and Engineering Centers, the Keck Foundation, the State of Illinois, and Northwestern University. Imaging studies were done at the Nikon Imaging Center, Feinberg School of Medicine, Northwestern University.

- Ethier CR (2002) The inner wall of Schlemm's canal. *Exp Eye Res* 74(2):161–172.
- Johnson M (2006) 'What controls aqueous humour outflow resistance?'. *Exp Eye Res* 82(4):545–557.
- Allingham RR, et al. (1992) The relationship between pore density and outflow facility in human eyes. *Invest Ophthalmol Vis Sci* 33(5):1661–1669.
- Johnson M, et al. (2002) The pore density in the inner wall endothelium of Schlemm's canal of glaucomatous eyes. *Invest Ophthalmol Vis Sci* 43(9):2950–2955.
- Pedrigi RM, Simon D, Reed A, Stamer WD, Overby DR (2011) A model of giant vacuole dynamics in human Schlemm's canal endothelial cells. *Exp Eye Res* 92(1):57–66.
- Stamer WD, Roberts BC, Howell DN, Epstein DL (1998) Isolation, culture, and characterization of endothelial cells from Schlemm's canal. *Invest Ophthalmol Vis Sci* 39(10):1804–1812.
- Perkumas KM, Stamer WD (2012) Protein markers and differentiation in culture for Schlemm's canal endothelial cells. *Exp Eye Res* 96(1):82–87.
- Ethier CR, Coloma FM, Sit AJ, Johnson M (1998) Two pore types in the inner-wall endothelium of Schlemm's canal. *Invest Ophthalmol Vis Sci* 39(11):2041–2048.
- Pederson JE, MacLellan HM, Gaasterland DE (1978) The rate of reflux fluid movement into the eye from Schlemm's canal during hypotony in the rhesus monkey. *Invest Ophthalmol Vis Sci* 17(4):377–381.
- Vargas-Pinto R, Gong H, Vahabikashi A, Johnson M (2013) The effect of the endothelial cell cortex on atomic force microscopy measurements. *Biophys J* 105(2):300–309.
- Guo M, et al. (2013) The role of vimentin intermediate filaments in cortical and cytoplasmic mechanics. *Biophys J* 105(7):1562–1568.
- Byfield FJ, et al. (2009) Absence of filamin A prevents cells from responding to stiffness gradients on gels coated with collagen but not fibronectin. *Biophys J* 96(12):5095–5102.
- Solon J, Leventhal I, Sengupta K, Georges PC, Janmey PA (2007) Fibroblast adaptation and stiffness matching to soft elastic substrates. *Biophys J* 93(12):4453–4461.
- Hoffman BD, Massiera G, Van Citters KM, Crocker JC (2006) The consensus mechanics of cultured mammalian cells. *Proc Natl Acad Sci USA* 103(27):10259–10264.
- Zhou EH, et al. (2012) Mechanical responsiveness of the endothelial cell of Schlemm's canal: Scope, variability and its potential role in controlling aqueous humour outflow. *J R Soc Interface* 9(71):1144–1155.
- Last JA, et al. (2011) Elastic modulus determination of normal and glaucomatous human trabecular meshwork. *Invest Ophthalmol Vis Sci* 52(5):2147–2152.
- Liu F, et al. (2010) Feedback amplification of fibrosis through matrix stiffening and COX-2 suppression. *J Cell Biol* 190(4):693–706.
- Schlunck G, et al. (2008) Substrate rigidity modulates cell matrix interactions and protein expression in human trabecular meshwork cells. *Invest Ophthalmol Vis Sci* 49(1):262–269.
- Dupont S, et al. (2011) Role of YAP/TAZ in mechanotransduction. *Nature* 474(7350):179–183.
- Junglas B, et al. (2012) Connective tissue growth factor causes glaucoma by modifying the actin cytoskeleton of the trabecular meshwork. *Am J Pathol* 180(6):2386–2403.
- Leber T (1873) Studien über den Flüssigkeitswechsel im Auge. *Albrecht Von Graefes Arch Ophthalmol* 19:87–106.
- Keller KE, Acott TS (2013) The juxtacanalicular region of ocular trabecular meshwork: A tissue with a unique extracellular matrix and specialized function. *J Ocul Biol* 1(1):3.
- Johnson M, Shapiro A, Ethier CR, Kamm RD (1992) Modulation of outflow resistance by the pores of the inner wall endothelium. *Invest Ophthalmol Vis Sci* 33(5):1670–1675.
- Overby DR, Stamer WD, Johnson M (2009) The changing paradigm of outflow resistance generation: Towards synergistic models of the JCT and inner wall endothelium. *Exp Eye Res* 88(4):656–670.
- Lütjens-Drecoll E, Futa R, Rohen JW (1981) Ultrastructural studies on tangential sections of the trabecular meshwork in normal and glaucomatous eyes. *Invest Ophthalmol Vis Sci* 21(4):563–573.
- Camras LJ, Stamer WD, Epstein D, Gonzalez P, Yuan F (2014) Circumferential tensile stiffness of glaucomatous trabecular meshwork. *Invest Ophthalmol Vis Sci* 55(2):814–823.
- Chen J, Runyan SA, Robinson MR (2011) Novel ocular antihypertensive compounds in clinical trials. *Clin Ophthalmol* 5:667–677.
- Williams RD, Novack GD, van Haarlem T, Kocpzyński C, AR-12286 Phase 2A Study Group (2011) Ocular hypotensive effect of the Rho kinase inhibitor AR-12286 in patients with glaucoma and ocular hypertension. *Am J Ophthalmol* 152(5):834–841, e1.
- Tian B, Geiger B, Epstein DL, Kaufman PL (2000) Cytoskeletal involvement in the regulation of aqueous humor outflow. *Invest Ophthalmol Vis Sci* 41(3):619–623.
- Rao VP, Epstein DL (2007) Rho GTPase/Rho kinase inhibition as a novel target for the treatment of glaucoma. *BioDrugs* 21(3):167–177.
- Fabry B, et al. (2001) Selected contribution: Time course and heterogeneity of contractile responses in cultured human airway smooth muscle cells. *J Appl Physiol* (1985) 91(2):986–994.
- Fabry B, et al. (2003) Time scale and other invariants of integrative mechanical behavior in living cells. *Phys Rev E Stat Nonlin Soft Matter Phys* 68(4 Pt 1):041914.
- Zhou EH, et al. (2009) Universal behavior of the osmotically compressed cell and its analogy to the colloidal glass transition. *Proc Natl Acad Sci USA* 106(26):10632–10637.
- Fabry B, et al. (2001) Scaling the microrheology of living cells. *Phys Rev Lett* 87(14):148102.
- Engler AJ, Sen S, Sweeney HL, Discher DE (2006) Matrix elasticity directs stem cell lineage specification. *Cell* 126(4):677–689.
- de Rooij J, Kerstens A, Danuser G, Schwartz MA, Waterman-Storer CM (2005) Integrin-dependent actomyosin contraction regulates epithelial cell scattering. *J Cell Biol* 171(1):153–164.
- McKee CT, et al. (2011) The effect of biophysical attributes of the ocular trabecular meshwork associated with glaucoma on the cell response to therapeutic agents. *Biomaterials* 32(9):2417–2423.
- Wood JA, et al. (2011) Substratum compliance regulates human trabecular meshwork cell behaviors and response to latrunculin B. *Invest Ophthalmol Vis Sci* 52(13):9298–9303.
- Vandesompele J, et al. (2002) Accurate normalization of real-time quantitative RT-PCR data by geometric averaging of multiple internal control genes. *Genome Biol* 3(7):research0034.1–research0034.11.
- Krishnamoorthy K, Thomson J (2004) A more powerful test for comparing two Poisson means. *J Stat Plan Inference* 119(1):23–35.
- Gong H, Ruberti J, Overby D, Johnson M, Fredo TF (2002) A new view of the human trabecular meshwork using quick-freeze, deep-etch electron microscopy. *Exp Eye Res* 75(3):347–358.
- Riedl J, et al. (2008) Lifeact: A versatile marker to visualize F-actin. *Nat Methods* 5(7):605–607.
- Pagano M, Gauvreau K (2000) *Principles of Biostatistics* (Cengage Learning, Independence, KY), Vol 2.
- Mijailovich SM, Kojic M, Zivkovic M, Fabry B, Fredberg JJ (2002) A finite element model of cell deformation during magnetic bead twisting. *J Appl Physiol* 93(4):1429–1436.

Supporting Information

Overby et al. 10.1073/pnas.1410602111

SI Text

Schlemm's Canal Monolayer Perfusions and Pore Counting. *Detailed methods.* Schlemm's canal (SC) cells were seeded at confluence and cultured for 2 d in serum-containing culture medium on the external bottom-facing surface of a polystyrene filter membrane insert (Corning Transwell 3470; 0.4- μm -diameter track-etched pores), following previously described methods (1). The filter membrane insert was sealed with a conical silicone stopper (Versilic; VWR) and the cells were perfused with serum-free medium at 37 °C in a basal-to-apical direction at 0 (control), 2 or 6 mmHg. After 30 min, the cells were immersed in fixative [2.5% (vol/vol) glutaraldehyde and 2.0% (wt/vol) paraformaldehyde in PBS; TAAB Laboratories Equipment] while perfusion with serum-free medium continued for an additional 30 min. The perfusion was then stopped, and the membrane insert was disconnected from the perfusion system and immersed in fixative for an additional 30 min. Standard procedures for scanning electron microscopy were used to examine the pores on a JSM 6390 scanning electron microscope (JEOL). To determine whether pore formation depended on the direction of perfusion, one SC cell strain (SC67) was perfused in the reverse apical-to-basal direction. For these experiments, SC cells were seeded on the internal top-facing surface of the filter membrane, such that flow crossed the cell layer in the apical-to-basal direction when the filter membrane insert was interfaced with the perfusion system.

Pore area and density (number of pores per square millimeter) were quantified by sampling 12 randomly selected regions for each cell layer. Each region ($\sim 5,500 \mu\text{m}^2$) was imaged at 1,500 \times magnification using scanning electron microscopy and any pore-like feature was reimaged at 10,000 \times magnification. Pore counting was done in a masked fashion. Pores were defined as circular or elliptical openings through the cell layer with smooth edges (2, 3). Pores were characterized as transcellular (passing through an individual cell) or paracellular (intersecting the junction between two neighboring cells) as previously described (3).

Pore density. Transcellular and paracellular pore density increased with perfusion pressure for all three nonglaucomatous cell strains at 2 or 6 mmHg compared with unperfused controls at 0 mmHg ($P < 0.005$; Fig. S1 *A* and *B*). When the pressure drop was reversed to perfuse one cell strain (SC67) in the apical-to-basal direction at 6 mmHg, the paracellular pore density significantly decreased compared with basal-to-apical perfusion ($P < 10^{-6}$), whereas the decrease in transcellular pore density was not statistically significant. The increased subcortical stiffness in glaucomatous cell strains was significantly correlated with decreasing transcellular pore density ($P < 0.02$; Fig. S1*C*), with a borderline significant correlation with decreasing paracellular pore density ($P < 0.07$; Fig. S1*D*).

Pore area. The porosity (total pore area per unit cell area) increased significantly with perfusion pressure for all three normal cell strains when perfused in the basal-to-apical direction at 2 ($P < 0.019$) or 6 mmHg ($P < 0.004$) but not in the apical-to-basal direction at 6 mmHg ($P = 0.79$; SC67) relative to unperfused controls (Fig. S2*A*). In the three glaucomatous cell strains, porosity was markedly reduced compared with the three normal cell strains when perfused at 6 mmHg in the basal-to-apical direction ($P < 0.035$; Fig. S2*B*). The porosity seen in glaucomatous SC cell strains perfused at 6 mmHg was comparable to that of unperfused normal controls (Fig. S2 *A* and *B*).

For those two normal and three glaucomatous SC cell strains in which both cell stiffness and pore area were measured, increasing subcortical stiffness [measured by atomic force microscopy (AFM), 10- μm spherical tip] correlated with decreasing porosity ($P < 0.012$; Fig. S2*C*).

AFM Studies. Control studies. The AFM data as measured with both sharp and rounded tips were found to be non-Gaussian as determined using Q-Q plots (4) (Fig. S3 *A* and *B*). However, a log transformation of the data yielded a Gaussian distribution (Fig. S3 *C* and *D*) and thus the statistics used on the AFM data were done on log-transformed data.

Table S1 gives the P values (paired t test) for each tip geometry when comparing the mean values at the nuclear versus non-nuclear region for six normal and five glaucomatous strains. We concluded that there were no significant differences between AFM measurements in the nuclear and nonnuclear regions, similar to a conclusion we had drawn earlier on other endothelial cell types (5).

We investigated the possibility of a relationship between donor age and modulus as measured by AFM using the Pearson correlation coefficient. No such relationship was found (Table S2). Thus, even though the glaucomatous cell strains come from somewhat older individuals than do the normal cell strains, it is not likely that this can explain the difference between the AFM stiffnesses of normal and glaucomatous cells strains reported in this study.

Effect of latrunculin-A. To examine the contribution of the actin cytoskeleton to SC cell stiffness, normal and glaucomatous SC cells were treated with the actin-depolymerizing agent latrunculin-A, and then the cell stiffness was measured with AFM using sharp tips and larger rounded tips. Treatment led to complete depolymerization of the SC cell cortex and a very substantial reduction in stress fibers and fibrillar collagen (Fig. 3*A*); there was no apparent difference in filamentous actin distribution between normal and glaucomatous SC cells. Latrunculin-A caused a significant decrease in cell stiffness of both cortical and subcortical cytoskeleton in both normal and glaucomatous SC cells (Fig. S4), confirming the importance of actin to cell stiffness at both of these sites. There was no apparent difference in the relative decrease in cell stiffness caused by latrunculin-A when comparing normal to glaucomatous cells.

Optical Magnetic Twisting Cytometry Studies. Effect of cell passaging. We have previously evaluated the effect of cell passaging on the mechanical phenotype of SC cells (6). Cell stiffness, contractile response to FBS, and relaxing response to isoproterenol were relatively stable from passages 2–6.

AFM characterization of gels. A commercial AFM (MFP-3D; Asylum) was used with probes constructed with borosilicate spherical tips, nominal diameter 5 μm , glued to triangular Au-coated silicon nitride cantilevers with a nominal spring constant of 0.06 N/m (Novascan Technologies). Ten force-displacement curves were collected from each sample and used to determine gel modulus as a function of cross-linker concentration (Fig. S5). Maximum forces were set to ~ 1.5 nN.

Baseline studies. When SC cells were grown on a rigid substrate, we did not find any difference in their baseline cytoskeletal stiffness as measured using optical magnetic twisting cytometry (OMTC) between normal and glaucomatous SC cells (Fig. S6).

Effects of drugs that alter outflow resistance. We previously reported how normal SC cells respond differently to drugs with known effects on outflow resistance (6). Here we extend those results to glaucomatous SC cells. Sphingosine-1-phosphate (S1P), thrombin, and lysophosphatidic acid (LPA), all known to increase outflow resistance at the tissue level, promptly increased cell stiffness by up to 200% (Fig. S7). Conversely, latrunculin-A, isoproterenol, dibutyl cyclic-AMP (DBcAMP), or Y-27632, all known to decrease outflow resistance at the tissue level, dose-dependently decreased cell stiffness by up to 80% (Figs. S7 and S8). In the case of isoproterenol treatment, the lack of cytoskeletal softening correlated with the lack of $\beta 2$ adrenergic receptor expression (Fig. S8G), consistent with our previous finding on normal SC cells alone (6). These results also extended another previous finding—that drugs that modulate outflow resistance also modulate SC cell stiffness in tandem (6)—from normal to glaucomatous cells (i.e., glaucoma SC cells are also responsive to treatments known to affect outflow resistance).

Statistical methods for gene expression studies. The effect of cell strain donor age was examined by adding this as an extra covariate to the regression analysis:

$$\frac{\text{Variable}(E_{\text{Substrate}})}{\text{Variable}(1.1 \text{ kPa})} - 1 = b_1 * \left(\frac{E_{\text{Substrate}}}{1.1 \text{ kPa}} - 1 \right) + b_2 * \left(\frac{E_{\text{Substrate}}}{1.1 \text{ kPa}} - 1 \right) * \text{Normal} + b_3 * \left(\frac{E_{\text{Substrate}}}{1.1 \text{ kPa}} - 1 \right) * \text{Age}.$$

Only for three genes did this have any effect on the conclusions from the regression analysis. *MMP2* expression was found to decrease significantly with cell strain donor age ($P < 0.001$), to increase with substrate stiffness ($P < 10^{-4}$), and not to be affected by glaucoma ($P > 0.5$). *PAII* was also found to decrease significantly with cell strain donor age ($P < 0.005$), to increase with substrate stiffness ($P < 0.02$), and not to be affected by glaucoma ($P > 0.5$). The marginally significant negative association with substrate stiffness in glaucomatous cells for *PTGS2* was not distinguishable from a marginally significant negative association with aging.

Real-Time Quantitative PCR. The sequences of primers used are shown in Table S3.

- Pedrigi RM, Simon D, Reed A, Stamer WD, Overby DR (2011) A model of giant vacuole dynamics in human Schlemm's canal endothelial cells. *Exp Eye Res* 92(1):57–66.
- Sit AJ, Coloma FM, Ethier CR, Johnson M (1997) Factors affecting the pores of the inner wall endothelium of Schlemm's canal. *Invest Ophthalmol Vis Sci* 38(8): 1517–1525.
- Ethier CR, Coloma FM, Sit AJ, Johnson M (1998) Two pore types in the inner-wall endothelium of Schlemm's canal. *Invest Ophthalmol Vis Sci* 39(11):2041–2048.
- Moore D, McCabe G, Craig B (2009) *Introduction to the Practice of Statistics* (Freeman, New York), 6th Ed, pp 417–486.
- Vargas-Pinto R, Gong H, Vahabikashi A, Johnson M (2013) The effect of the endothelial cell cortex on atomic force microscopy measurements. *Biophys J* 105(2):300–309.
- Zhou EH, et al. (2012) Mechanical responsiveness of the endothelial cell of Schlemm's canal: Scope, variability and its potential role in controlling aqueous humour outflow. *J R Soc Interface* 9(71):1144–1155.

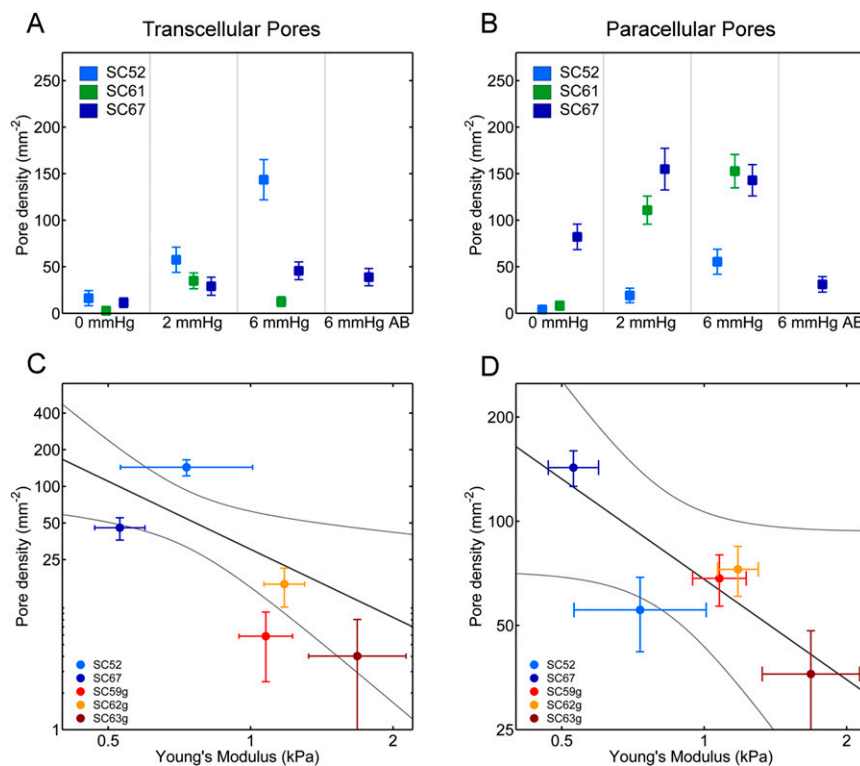


Fig. S1. Effects of pressure drop and subcortical stiffness on transcellular and paracellular pore density (number of pores per unit cell area). (A) Transcellular pore density increases in nonglaucomatous SC cell strains when perfused in the basal-to-apical direction at 2 or 6 mmHg ($P < 0.002$) relative to unperfused controls at 0 mmHg. (B) Paracellular pore density increases at 2 or 6 mmHg ($P < 0.005$) relative to 0 mmHg unperfused controls. Reversing the pressure drop in one SC cell strain (SC67) decreased the paracellular ($P < 10^{-6}$), but not transcellular, pore density. (C) There is a significant correlation (dark line) between decreasing transcellular pore density and increasing subcortical Young's modulus measured by AFM with 10- μm spherical tips ($P < 0.02$). (D) There is a borderline significant correlation (dark line) between decreasing paracellular pore density and increasing subcortical Young's modulus ($P < 0.07$). Bars represent SEM on pore density and modulus. Light curves in C and D represent 95% confidence intervals on the slope of the generalized linear model (GLM) linear regression.

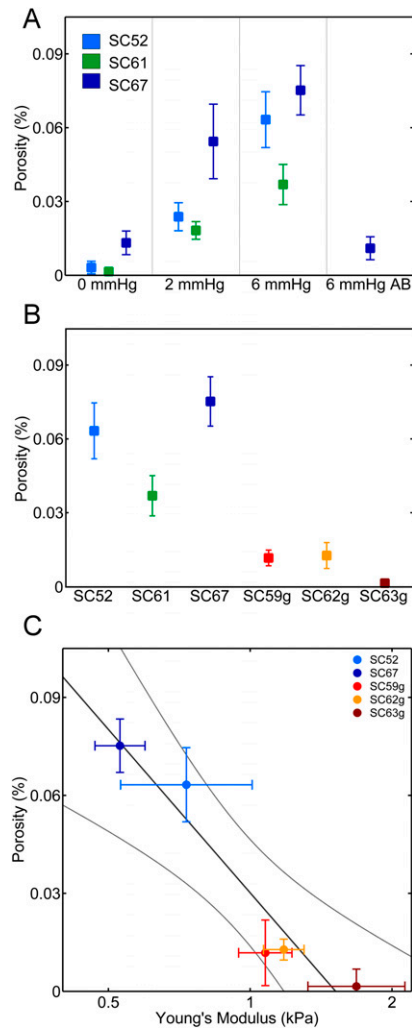


Fig. S2. Effects of pressure and glaucoma on porosity (pore area per unit cell area). (A) Porosity increases in three nonglaucomatous SC cell strains as a function of pressure drop in the basal-to-apical direction at 0, 2, or 6 mmHg. In the one SC cell strain (SC67) perfused in the apical-to-basal direction (AB) at 6 mmHg, porosity is similar to the unperfused controls at 0 mmHg. (B) Porosity is less in glaucomatous (SC59g, SC62g, and SC63g) compared with normal SC cells (SC52, SC 61, and SC67) following perfusion at 6 mmHg in the basal-to-apical direction. (C) There is a significant correlation (dark curve) between decreasing porosity and increasing Young's modulus as measured by AFM with 10- μ m spherical tips. Bars represent SEM on porosity and modulus. Light curves in C represent 95% confident intervals on the slope of the GLM linear regression.

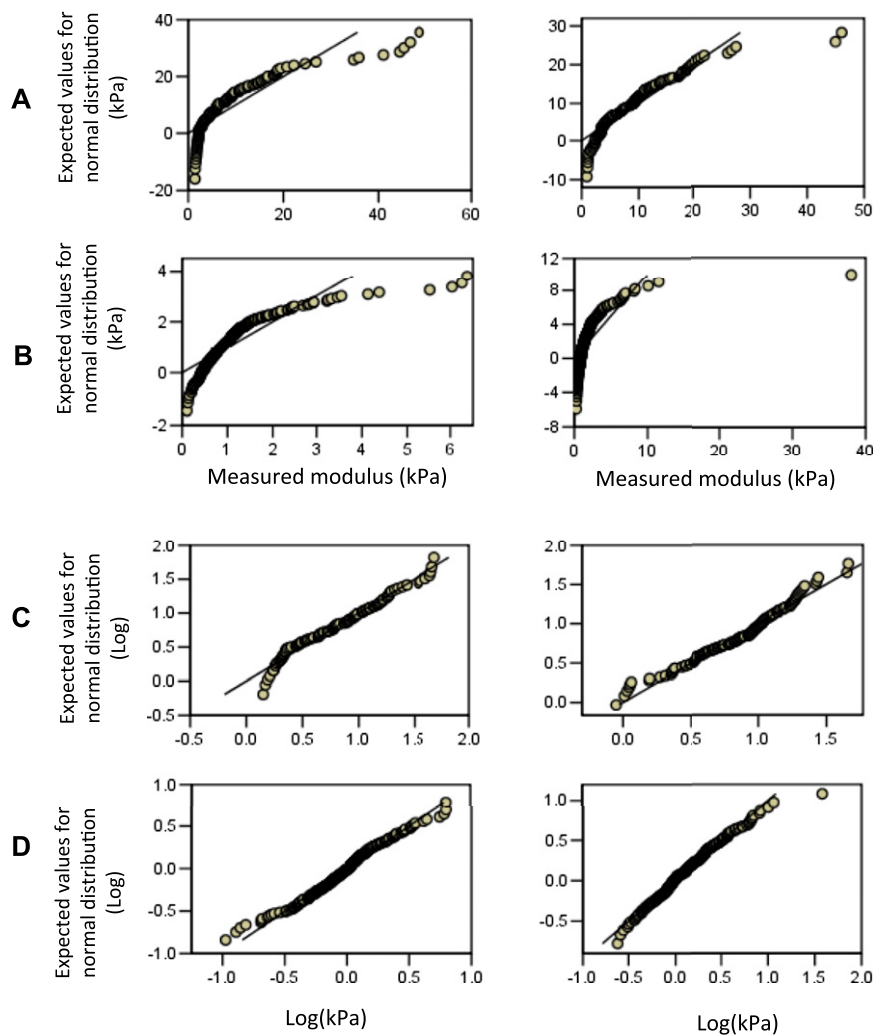


Fig. S3. Q-Q plots for AFM data. Plots compare the quantiles for the Young's modulus measured to the expected values if data follow a normal distribution. Left panels are for normal SC cells (SC41, SC51, SC52, SC58, SC60, and SC67); right panels are for glaucomatous SC cells (SC57, SC59, SC62, SC63, and SC64). (A) AFM modulus measurements using sharp tips. (B) AFM data measurements with 4.5- and 10- μm spherical tips. (C) AFM measurements with sharp tips after logarithmic transformation. (D) AFM data measurements with spherical tips after logarithmic transformation. All datasets follow a Gaussian distribution after the transformation.

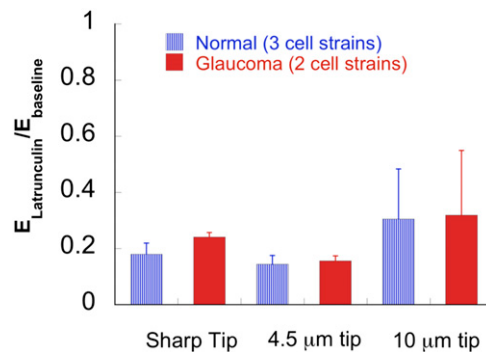


Fig. S4. Decrease in cell stiffness following latrunculin-A as measured by AFM. The ratio of the cell modulus measured after 30 min of treatment with latrunculin-A (1 μM) ($E_{\text{latrunculin}}$) compared with the cell modulus measured immediately before treatment with latrunculin (E_{baseline}) in the same population of cells. Measurements performed in two normal and three glaucomatous cell strains.

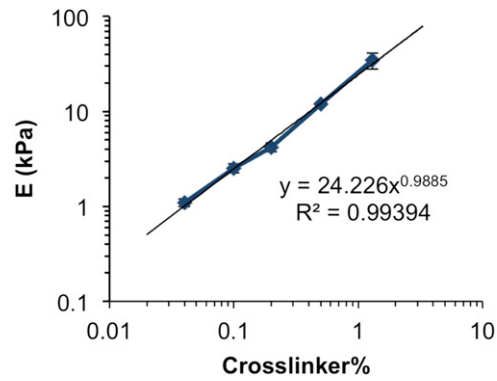


Fig. S5. Effect of cross-linker concentration on the stiffness of gels, measured using AFM. Mean \pm SEM, $n = 10$ per data point.

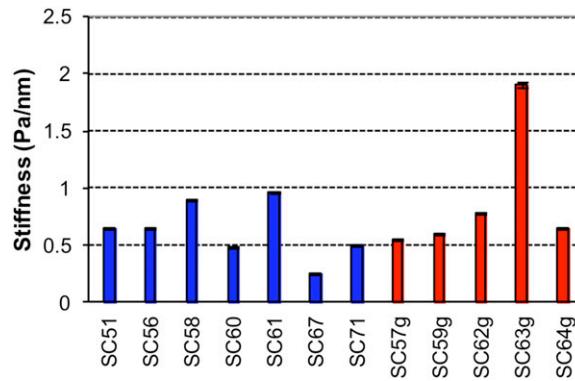


Fig. S6. Comparison of cell stiffness as measured by OMTC between normal and glaucomatous SC cells grown on rigid substrates. Cell stiffness (g) was measured using OMTC with cells grown on collagen-coated plastic as described previously (6). Median \pm SEM with $n > 3,746$ beads for each donor; $P = 0.3$ by t test between normal ($n = 7$) and glaucoma strains ($n = 5$). Data for SC51, SC56, SC58, SC60, and SC61 were from our previous work (6) and are included here for comparison.

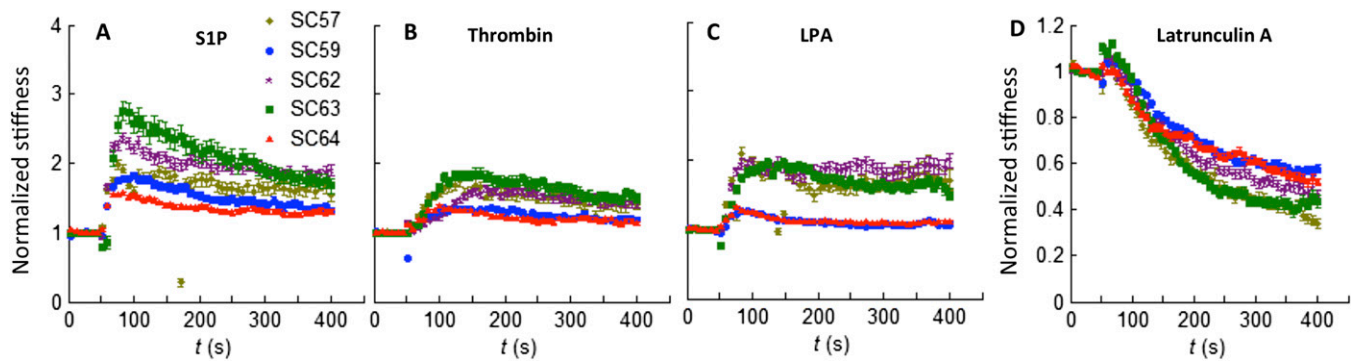


Fig. S7. The evolution of cell stiffness with time was monitored using OMTC while the indicated drug was introduced at ~ 50 s, as described previously (6). Similar to normal SC cells (6), glaucomatous SC cells contracted in response to S1P (A), thrombin (B), and LPA (C) and relaxed in response to latrunculin-A (D). Cell stiffness was normalized by predrug control. Median \pm SEM with $n > 300$ beads for each data series. When we compared drug response at 300 s, there was no difference between normal ($n = 5$) (6) and glaucoma ($n = 5$); $P > 0.43$.

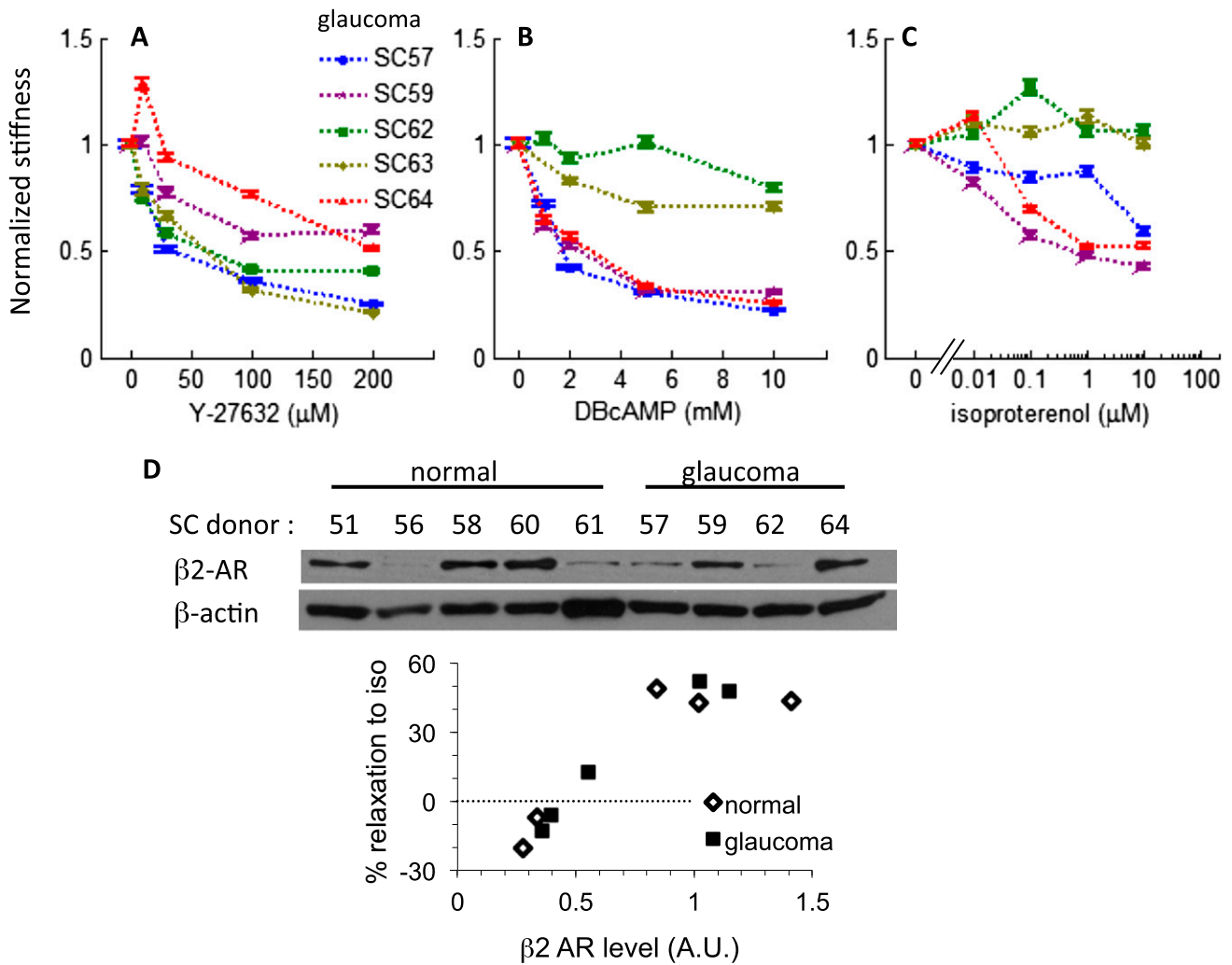


Fig. 58. The dose-dependent relaxation of SC cells was quantified using OMTC after \sim 45-min incubation with the indicated drug, as described previously (6). Similar to normal SC cells (6), glaucomatous cells also dose-dependently relaxed in response to Y-27632 (A), DBcAMP (B), and isoproterenol (C) in a donor-dependent manner. Median \pm SEM with $n > 1,000$ beads for each data point. When we compared drug response at each dose for each drug, there was no difference between normal ($n = 5$) (6) and glaucoma ($n = 5$); $P > 0.26$. (D) The protein level of β 2 adrenergic receptor was quantified using Western blot (Upper); the protein of SC63 was run on another blot and not shown. Protein level was positively correlated with the relaxation response to $1 \mu\text{M}$ isoproterenol (Lower). Data for normal SC cells were from our previous work (6) and are included here for comparison.

Table S1. Nucleus versus nonnuclear AFM measurements

AFM tip	<i>P</i> value for normal lines ($n = 6$)	<i>P</i> value for glaucomatous lines ($n = 5$)
Sharp	0.655 ($m = 104$)	0.071 ($m = 148$)
4.5- μm sphere	0.212 ($m = 104$)	0.928 ($m = 122$)
10- μm sphere	0.101 ($m = 153$)	0.735 ($m = 111$)

Paired *t* test, nucleus vs. cytoplasm. *m*, number of measurements.

Table S2. Correlation coefficient (*r*) of AFM measurement with donor age

AFM tip and cell strains	<i>r</i>	<i>P</i> value
4.5- μ m sphere, all strains	-0.02	0.960
Normals (<i>n</i> = 6, <i>m</i> = 104)	-0.56	0.247
Glaucomas (<i>n</i> = 5, <i>m</i> = 128)	-0.19	0.759
10- μ m sphere, all strains	0.33	0.329
Normals (<i>n</i> = 6, <i>m</i> = 153)	-0.28	0.590
Glaucomas (<i>n</i> = 5, <i>m</i> = 120)	0.50	0.396
Sharp tip, all strains	0.39	0.235
Normals (<i>n</i> = 6, <i>m</i> = 104)	0.29	0.577
Glaucomas (<i>n</i> = 5, <i>m</i> = 148)	0.65	0.236

m, number of measurements; *n*, number of cells.

Table S3. Sequences of primers used for real-time RT-PCR

Gene	Sequence	Position
<i>GAPDH</i>	5'-AGCCACATCGCTCAGACA-3'	83-148
	5'-GCCCAATACGACCAAATCC-3'	
<i>GNB2L</i>	5'-GCTACTACCCCGCAGTTC-3'	170-241
	5'-CAGTTTCCACATGATGATGGTC-3'	
<i>MMP2</i>	5'-ATAACCTGGATGCCGTCGT-3'	2148-2210
	5'-AGGCACCCTTGAAGAAGTAGC-3'	
<i>PAI1</i>	5'-AAGGCACCTCTGAGAACTCA-3'	53-113
	5'-CCCAGACTAGGCAGGTG-3'	
<i>CTGF</i>	5'-CTCCTGCAGGCTAGAGAAGC-3'	884-977
	5'-GATGCACTTTTGGCCCTTCTT-3'	
<i>COL1A1</i>	5'-GGGATTCCTTGGACCTAAAG-3'	1869-1928
	5'-GGAACACCTCGCTCTCCA-3'	
<i>SPARC</i>	5'-GTGCAGAGGAAACCGAAGAG-3'	376-439
	5'-TGTTTGCAGTGGTGGTTCTG-3'	
<i>TGM2</i>	5'-GGCACCAAGTACCTGCTCA-3'	1673-1742
	5'-AGAGGATGCAAAGAGGAACG-3'	
<i>TPM1</i>	5'-TGGATCAGACCTTGAAAGCA-3'	790-880
	5'-TCGGAAGGACCTTGATCTC-3'	
<i>PTGS2</i>	5'-TGGAAGCCTTCTTAACCTC-3'	512-613
	5'-TCAGGAAGCTGCTTTTACCTT-3'	
<i>ACTA2</i>	5'-CTGTTCCAGCCATCCTTCAT-3'	1262-1331
	5'-TCAGGAAGCTGCTTTTACCTT-3'	
<i>TGF-B2</i>	5'-CCAAAGGGTACAATGCCAAC-3'	1194-1283
	5'-CAGATGCTTCTGGATTTATGGTATT-3'	
<i>DCN</i>	5'-ATGCAGCTAGCCTGAAAGGA-3'	1118-1199
	5'-GAGCCATTGTCAACAGCAGA-3'	
<i>BMP4</i>	5'-CTGCAACCGTTCAGAGGTC-3'	225-315
	5'-TGCTCGGGATGGCACTAC-3'	
<i>GREM1</i>	5'-GTGACGGAGCGCAAATACC-3'	406-509
	5'-CCTTCCTCGTGGATGGTCT-3'	